Twin-chain polymer hydrogels based on poly(vinyl alcohol) as new advanced tool for the cleaning of modern and contemporary art

Rosangela Mastrangelo[a,b], David Chelazzi[a,b], Giovanna Poggi[a,b], Emiliano Fratini[a,b], Luciano Pensabene Buemi[c], Maria Laura Petruzzellis[c], and Piero Baglioni[a,b,1]

[a]Department of Chemistry, University of Florence, I-50019 Florence, Italy; [b]Consorzio Interuniversitario per lo Sviluppo dei Sistemi a Grande Interfase (Center for Colloid and Surface Science), University of Florence, I-50019 Florence, Italy; and [c]Conservation Department, Peggy Guggenheim Collection, Dorsoduro 701, I-30123 Venice, Italy

Conservation of our cultural heritage is fundamental for conveying to future generations our culture, traditions, and ways of thinking and behaving. Cleaning art, in particular modern/contemporary paintings, with traditional tools could be risky and impractical, particularly on large collections of important works to be transferred to future generations. We report on advanced cleaning systems, based on twin-chain polymer networks made of poly(vinyl alcohol) (PVA) chains, semiinterpenetrated (semi-IPN) with PVA of lower molecular weight (L-PVA). Interpenetrating L-PVA causes a change from gels with oriented channels to sponge-like semi-IPNs with disordered interconnected pores, conferring different gel (and solvent) dynamics. These features grant residue-free, time efficient cleaning capacity and effective dirt capture, defeating risks for the artifact, making possible a safer treatment of important collections, unconceivable with conventional methods. We report as an example the conservation of Jackson Pollock's masterpieces, cleaned in a controlled way, safety and selectivity with unprecedented performance.

poly(vinyl alcohol) hydrogel | semiinterpenetrated gels networks | cultural heritage conservation | modern art | contemporary art

The challenge in the conservation of cultural heritage is to preserve and maintain accessible a vast number of objects (e.g., up to million artifacts for a single museum) against degradation caused by environmental factors, pollution, wrong conservation practice, and microorganisms. Heritage conservation and accessibility are both an economic amplifier and an invaluable instrument that drives social inclusion and equality, improving quality of life (1–3). The most recurrent issue in the preservation of modern and contemporary art involves the removal of soil from painted surfaces. This is often problematic owing to the fact that industrial paints contain additives (4, 5) with a marked sensitiveness to solvents and cleaning fluids (6, 7) that can possibly leach and deteriorate the painting. Since most contemporary paintings are unvarnished, soil accumulates directly on the painted layers, and cleaning solvents work in contact with sensitive pigments, dyes, binders, and additives. Moreover, especially from the 1940s on, paintings display high surface roughness, which makes homogeneous cleaning with traditional tools even more difficult and risky for the artifacts. In particular, the use of solvents is uncontrolled and nonselective, i.e., sensitive original components of the artifacts can be swollen, solubilized, or leached along with undesired layers. Besides, free solvents typically used in the restoration practice pose health risks to conservators. Traditionally employed solvent thickeners, such as polyacrylic acid and cellulose derivatives, or physical gels (e.g., agar), can either be scarcely retentive or exhibit poor mechanical properties, leaving polymer residues whose removal requires invasive rinsing steps (8, 9).

In past years, we have developed a different approach based on the use of colloidal systems (10–17). The latest advancement is represented by the confinement of cleaning fluids in gels (18–20) specifically tailored to treat water- and solvent-sensitive works of art. In a previous contribution to PNAS (21), we reported on the use of semiinterpenetrated networks (SIPNs) of poly(2-hydroxyethyl methacrylate) and poly(vinylpyrrolidone) (pHEMA/PVP) to confine oil-in-water microemulsions and gradually release them on sensitive surfaces. This allows the safe removal of detrimental pressure-sensitive tapes and adhesives from paper artworks. However, while the pHEMA/PVP SIPNs are highly retentive and effective on flat surfaces, they are not able to adapt to rough, clotted, and three-dimensional (3D) textured surfaces, such as those of modern and contemporary paints by Van Gogh, Picasso, Pollock, and others. For this reason, we designed a class of gels, based on poly(vinyl alcohol) (PVA). Freeze–thaw (FT) PVA gels can be feasibly formulated to exhibit excellent strength and elasticity, with no need of toxic cross-linkers, as largely reported in the literature (22, 23). A significant advantage with respect to the aforementioned pHEMA chemical networks is that physical networks of PVA are highly viscoelastic, meaning that gel sheets can be made flexible while retaining optimal elongability and resistance to mechanical stress. Besides, PVA is biocompatible and nontoxic. The challenge is to design PVA networks with cohesive structure, adaptability to rough surfaces, high and interconnected porosity, and high water content and retentiveness. These are key features to boost the removal of dirt from artistic surfaces and can be more easily achieved when two different types of PVA are combined in a network. Interpenetrating

Significance

From the earliest cave paintings of mankind, to Renaissance frescos and modern art masterpieces, the preservation of surfaces against soiling and degradation is fundamental to transfer such a vast heritage to future generations. However, traditional cleaning methods are often invasive and risky. We overcame these limitations by designing a cleaning system in the framework of colloid and materials science. We formulated twin-chain hydrogels with ideal mechanical properties, retentiveness, and interconnected porosity, allowing adhesion to rough and textured paint layers, and controlled wetting of surfaces, granting safe removal of soil. The gels were used to clean two Jackson Pollock masterpieces, recovering their visual aspect, marking a turning point in the field of conservation of important collections worldwide.

CHEMISTRY

SOCIAL SCIENCES

the network of a higher molecular weight PVA (H-PVA) with PVA of lower molecular weight (L-PVA) is expected to impact the pores size and structure and the mechanical properties of the gels. Namely, we hypothesized that L-PVA could remain at least partially entangled in the H-PVA network, interposing between H-PVA chains, possibly altering the formation of walls and pores and changing the rheological properties of the network. Controlling the pore size distribution and the rheological behavior of the gels would allow to optimize the adhesion of the gel to the surface or the capture and transport of matter through the gel matrix.

We report a detailed picture of the formation mechanism of these twin-chain polymer network hydrogels (TC-PNs) and of the PVA dynamics in the final network. We demonstrated that the addition of L-PVA changes the gel porosity from a packed structure of elongated channels into a nonordered pattern of interconnected and larger pores similar to a sponge. The morphological changes and the presence of L-PVA likely make the TC-PNs more mechanically compliant. These combined features grant higher cleaning efficacy than pure PVA networks and overcome the limitations of rigid gel sheets (e.g., gellan) and previously developed SIPNs (chemically cross-linked networks).

The advanced TC-PNs were used for the cleaning and conservation of two Pollock masterpieces from the Peggy Guggenheim Collection of Venice (Solomon R. Guggenheim Foundation, New York). The gels allowed safe removal of soil without uncontrolled spreading and excessive wetting of the painted layers. The gels do not leave residues and can be applied to vertical surfaces and then completely removed even from cracked and morphologically complex areas, reducing the risk of mechanical stresses. This is a dramatic improvement over the traditional cleaning approach with nonconfined solvents, which can require a long process under the microscope.

Results and Discussion

The Structure of PVA-Based Cryogels. In this contribution, PVA-based FT hydrogels were cryoformed: pure PVA hydrogels were prepared using H-PVA, and TC-PNs were obtained by mixing H-PVA and L-PVA. The terms TC-PNs and PVA/PVA gels will be used hereafter interchangeably. Hydrogels were either prepared with one (FT1) or three (FT3) FT cycles. The physical gelation of PVA solutions is driven by the freezing steps, which cause a water–polymer phase separation (22). PVA chains accumulate in the polymer-rich phase, while ice crystals form in the water-rich phase; owing to the pressure exerted by freezing water, polymer crystallites form and act as tie points in the gel structure, while ice crystals act as porogens. More details about the preparation are reported in *SI Appendix*. Confocal microscopy and scanning electron microscopy (SEM) were used to characterize the hydrogels. The freezing of H-PVA solutions leads to a more homogeneous structure with smaller pores than the TC-PNs (Fig. 1*A*). The pores are arranged into a pseudo-hexagonal packed structure (see detail of the β-plane section in Fig. 1*A*). The formation of the PVA gel walls follows the dendritic growth of ice during crystallization: there is a central branch from which new ice strands originate and arrange perpendicular to each other (Fig. 1*A*, α-plane section). As a consequence, pores have an elongated shape and exhibit an elliptical section, as if ice grew in aligned needles along axes that are slightly tilted with respect to the plane of the gel sheet's main surface (Fig. 1*A*). Instead, in the TC-PNs, pores are not aligned along axes and show a nonordered pattern similar to what is expected for a sponge-like network (Fig. 1*B*). The dimensions and distribution of the pores in the TC-PNs (3 to 30 μm) suggest the presence of obstacles that prevent the growth of ice, resulting in an interconnected porosity across the gel network. We hypothesized that this feature might favor the capture and retaining of dirt by the TC-PN gels: when the gel is applied on a soiled surface, the soil migrates inside the porosity, all through the gel volume; evaporation at the gel upper surface is expected to recall water from the bulk through the interconnected porosity, favoring dirt pick-up. Dirt capture should also be favored by the larger pore dimensions in the TC-PNs.
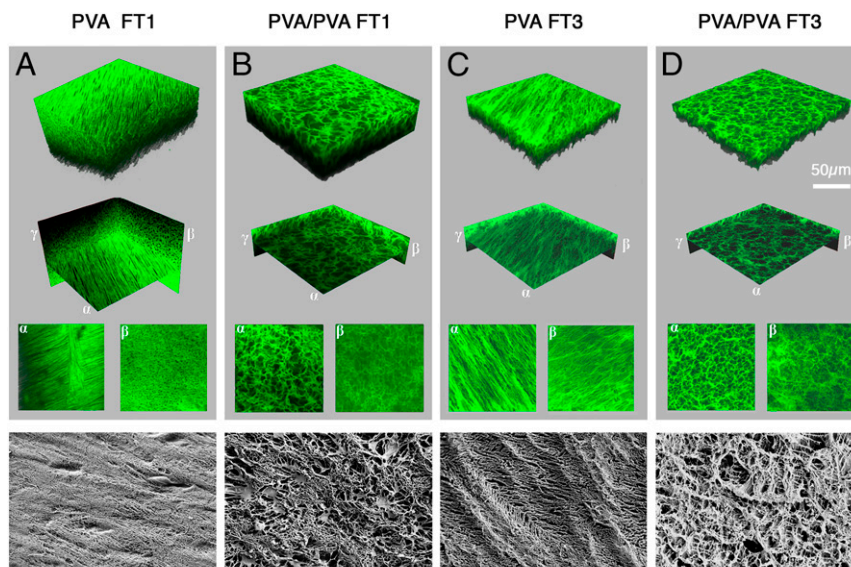

Fig. 1. The structure of PVA cryogels at the micron scale. Confocal-microscopy images of the FT PVA gels, loaded with an aqueous solution of the green dye rhodamine 110, which preferentially interacts with the gel's walls. *A–D* also include images of horizontal (α) and vertical (β and γ) sections of the imaged volumes. (*A*) PVA FT1 gel. The pores are cylindrical and arranged into a hexagonally packed structure (see detail of the β-plane section), with central branches from which new strands originate and arrange perpendicular to each other (see detail of the α-plane section). (*B*) TC-PN FT1 gel. The presence of L-PVA as semiinterpenetrated polymer leads to the formation of larger and nonoriented pores; the pore distribution resembles that of a sponge-like network (see sections along the α and β planes) (*C*) PVA FT3 gel. (*D*) TC-PN FT3 gel. In both FT3 hydrogels, the pores walls are thicker, as repeated FT cycles cause further phase separation, increasing local polymer concentration. The bottom row in *A–D* shows SEM images of xerogels obtained from the PVA-based gels, highlighting the presence of a wide range of pores' diameters in TC-PNs (*B* and *D*), including pores <1 μm. Bar dimension is 20 μm.

The strong directional growth of the pores in the pure PVA network is also evident when the number of FT cycles is higher, and the pores' section is larger, owing to the ice expansion during the second and third freezing steps (24) (Fig. 1C). Some of the pores merge together, resulting in a less orderly packed structure (24) than FT1 (Fig. 1C, α and β sections). For what concerns the TC-PNs, the FT3 network exhibits a similar disordered sponge-like pattern, suggesting that the TC-PN conserves its structure after the first cycle (Fig. 1D).

In both FT3 hydrogels the pores walls are thicker, because repeated cycles cause further phase separation, squeezing water out of the liquid-like portions of the gels' walls and increasing local polymer concentration (22). This is in agreement with the higher gel fraction (G%) reported in *SI Appendix*, Table S1. Small-angle X-ray scattering (SAXS) analysis shows that with increasing FT cycles, gel walls become denser also at the nanoscale, as evidenced by the decrease of the correlation lengths, and by the higher number of PVA crystallites, as shown by changes in the ratio between the Guinier scale (I_G) and the Lorentz scale (I_L) (*SI Appendix*, Table S2 and Fig. S1).

The SEM images of xerogels confirm that the pure PVA gels have an ordered pore structure (Fig. 1 A and C), while PVA/PVA xerogels show the same disordered, sponge-like porosity observed for the hydrogels in confocal images (see Fig. 3 B and C); the SEM images highlighted the presence of a wide range of pores' diameters in TC-PNs, including pores smaller than 1 μm.

A quantitative characterization of the confocal images was obtained performing chord-length distribution analysis (Fig. 2 and *SI Appendix*, Fig. S2). This method was firstly introduced by Tchoubar and Levitz (25, 26) and allows to extract stringent structural descriptors for biphasic media. Chords are defined as the segments that form when a set of randomly oriented lines cross phase boundaries. Fig. 2 A and B show the averaged frequency of chords with given length (f(R)) for both pores and gel-phases of the four confocal stacks (PVA and PVA/PVA, FT1, FT3). The distributions always show a peak and an exponential tail (27), from which a characteristic persistence length (λ) of the structure was obtained for each type of gel (*SI Appendix*, Table S3).
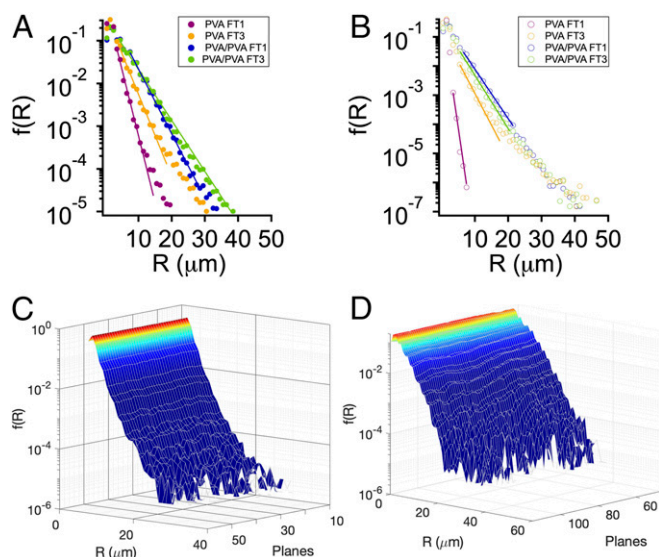

Fig. 2. Chord-length analysis of PVA cryogels. (A and B) Averaged chord-length distributions for the pore phase (A) and the gel phase (B) of PVA cryogels. The lines are the fitting of the data to exponential decays (*SI Appendix*). (C and D) The variance of chord distributions of pores with the depth of confocal stacks for PVA FT1 (C) and PVA/PVA FT1 (D).

The chord distributions of pores (Fig. 2A) show that λ increases with the number of FT cycles. In PVA/PVA samples, both the persistence length and the maximum pores' size are higher than the PVA gels, suggesting that L-PVA acts as a porogen in the final structure. The gels' walls thickness increases passing from PVA FT1 to PVA FT3 (Fig. 2B and *SI Appendix*, Table S3), and some further increase occurs passing from pure to PVA/PVA gels. It must be noticed that the higher thickness of walls in PVA/PVA FT3 as compared to PVA/PVA FT1, observed with SEM, could not be appreciated with chord analysis as the difference probably falls beyond the resolution of confocal images.

Fig. 2 C and D shows how the pore chord distribution varies along the depth of the stacks: all samples show a faster decay for confocal planes closer to the gel surface (see also *SI Appendix*, Fig. S3). This is probably due to the stronger effect of freezing on the exposed surfaces of the samples, which causes the formation of more elongated pores, while the inner planes are characterized by pores with larger cross-sections and polydispersity (*SI Appendix*, Fig. S2).

Gelation Mechanism of TC-PNs. The gelation mechanism of TC-PN FT1 was further studied with confocal microscopy, using labeled polymers to explain the difference in the hydrogel porosity with respect to the pure network. L-PVA was red-labeled with rhodamine B isothiocyanate (RBITC), while H-PVA was green-labeled with fluorescein isothiocyanate (FITC) (*SI Appendix*, section S1.3). Confocal images of the H-PVA/L-PVA pregel solution show the presence of 2- to 20-μm blobs, mainly composed of L-PVA (Fig. 3A). In the H-PVA solution, no such aggregates are detectable.

The phase separation in the H-PVA/L-PVA solution is an intriguing behavior that needs further comments.

In principle, the solubility of PVAs strongly depends on their hydrolysis degree, molecular weight, and crystallinity (28). According to the literature, both PVAs with a high (>95%) and low (87 to 89%) degree of hydrolysis are soluble in water at the conditions that we used for the preparation of the pregel solution (i.e., mixing at 98 °C and then cooling down to room temperature; *SI Appendix*, section S1.1) (29–31). Therefore, we do not ascribe the phase separation to poor solubility of either H-PVA or L-PVA in water. Phase separation was observed even using higher dissolution temperature (125 °C, close to the boiling temperature of the mixture). More information was gained from the phase diagrams reported in *SI Appendix*, Fig. S4. H-PVA does not show phase separation in the considered temperature and concentration ranges (5 to 100 °C and 3 to 15% wt/wt), while L-PVA, being less hydrolyzed, shows, according to the literature (32, 33), a lower critical solution temperature. The H-PVA/L-PVA mixtures, which are used to realize the gels presented in this paper, show a different behavior than the single-polymer solutions (*SI Appendix*, Fig. S4C). The confocal analysis of the mixtures is in agreement with a liquid–liquid polymer demixing that could be explained considering that, in the concentrated regime, H-PVA chains preferentially interact with each other, as a result of the polymer conformation in solution and of the high number of hydroxyl groups. According to Crowther et al. (34), the solvation of PVA after decoiling (T > 20 °C) appears to be hydrophilic in character with further increasing temperature. Budhlall et al. (35) confirmed via NMR that the interaction of R-OHs with water is temperature-dependent, while methyl protons associated with the acetate groups are more hydrophobic. Thus, in the pregel PVA solution, the highly hydrolyzed H-PVA is expected to be in the form of decoiled and solvated chains. Instead, partially hydrolyzed PVAs (such as L-PVA) adopt in solution different conformations, depending on the polymer blockiness, i.e., whether acetate blocks are long ("blocky") or randomly distributed ("less blocky"). Namely, blocky PVAs adopt a pseudomicelle conformation (with the acetate groups in a tight core and the
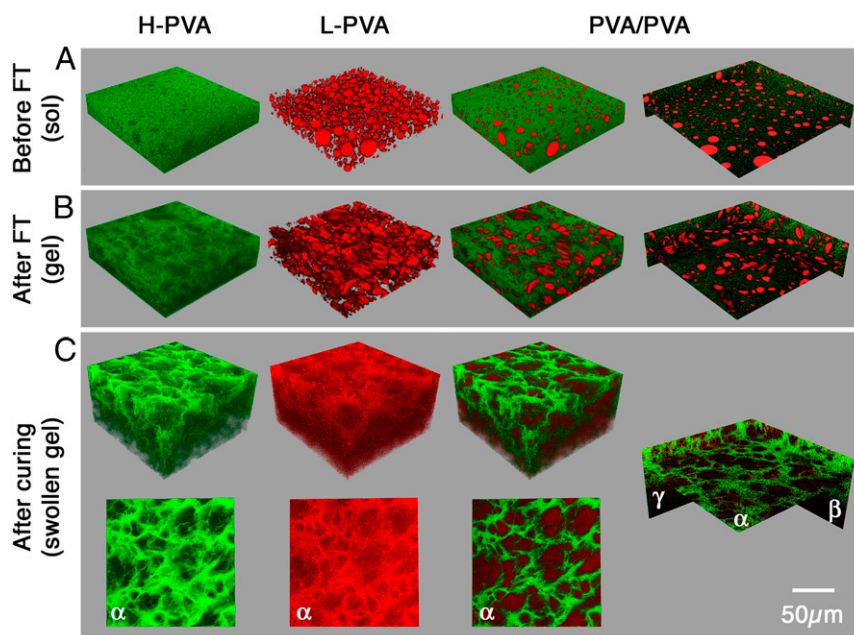
Fig. 3. Confocal-microscopy images of the PVA/PVA system. H-PVA is labeled in green with FITC and L-PVA in red with RBITC. Thus, the first column shows the FITC-PVA, the second column shows the RBITC-PVA, and the third and fourth columns show the sum of both components. (*A*) The PVA/PVA solution before the FT process. (*B*) The PVA/PVA gel network obtained after the FT process (1 cycle). The formation of ice crystals along preferential axes leads to the deformation of the blobs, which are distorted from spherical to elongated shapes; some of the smaller blobs coalesced together. (*C*) The PVA/PVA network after the first cycle of the FT process and 1 wk of curing in water. The 2D view of the top horizontal planes (α) highlights that L-PVA is preferentially localized on the gel's walls, interacting with the green-labeled H-PVA. L-PVA is also present inside the pores, throughout the gel volume.

highly solvated vinyl alcohol chains dangling in water), while less blocky polymers collapse on themselves in a denser conformation (35). Comparing the data obtained by Budhlall et al. with the hydrodynamic radius of L-PVA chains in extremely dilute solutions (R_H = 10.2 nm, obtained through the Stokes–Einstein equation using the diffusion coefficient [D] obtained by fluorescence correlation spectroscopy [FCS] measurements; D = 24 μm^2/s; *SI Appendix*, Table S4), we deduced that in our case L-PVA chains fall in the second type of behavior (collapsed structures). H-PVA–L-PVA interaction is probably not favored in the PVA/PVA pregel solution: decoiled H-PVA chains preferentially interact with each other through intermolecular H bonding, while L-PVA chains are collapsed and intramolecular hydrophobic interactions prevail. Therefore, L-PVA is expelled by the continuous phase of H-PVA and forms spherical droplets. As a matter of fact, the diffusion coefficient obtained by fluorescence recovery after photobleaching (FRAP) measurements in the blobs is significantly higher than that measured in the continuous phase (*SI Appendix*, Table S4), suggesting that the blob phase is less viscous, i.e., chains or aggregates in this phase are not strongly interacting with each other.

As previously mentioned, the physical crosslinking of PVA chains is driven by the freezing steps, applied to a PVA solution, which cause water–polymer phase separation and the formation of PVA crystallites that act as tie points in the structure. Ice crystals act as porogens in the process; therefore, ice formation plays a key role along with the H-PVA/L-PVA phase separation in the formation of the final network. In fact, the confocal images in Fig. 3 show that the L-PVA spherical blobs act as templates during the cryoformation of the TC-PN structure. Because L-PVA is more water soluble than H-PVA, it does not undergo further phase separation in the freezing step, thus remaining confined in the water pockets during freezing and after thawing. The formation of ice crystals along preferential axes leads to the deformation of the blobs from spherical to elongated shapes (36) (red features in Fig. 3*B*).

Typically, IPNs undergo both nucleation and growth and spinodal decomposition kinetics of phase separation (37). As a general rule, the most probable mechanism of phase separation is nucleation and growth for sequential IPNs, and spinodal decomposition for networks created by simultaneous formation from "monomers" or, in our case, preformed polymers (38). This, along with the role of ice as a porogen, would point in the direction of having nucleation and growth as the main mechanism for pore formation in the case of the FT TC-PNs. Indeed, nucleation and growth tend to produce spheres of the second phase in the matrix of the first phase, similarly to the structures observed with confocal microscopy, while spinodal decomposition produces interconnected cylinders of the second phase in the first phase matrix, even if coarsening and coalescence can cause significant structural changes at later stages (the final structure will be determined by the time at which the system loses its mobility). It must be also considered that, when phase separation occurs before gelation (as clearly shown in our case by confocal images), the phase domains will tend to be large, as gelation will tend to keep the domains apart (37); this is in good agreement with the large pore size observed for the FT TC-PNs. However, we cannot fully rule out that the gels can be described through an arrested spinodal decomposition driven by demixing of the two different polymers (39).

Washing the gels in water causes partial removal of L-PVA, leading the disordered and interconnected porous structure of the TC-PNs. However, confocal microscopy showed that the RBITC-labeled L-PVA is still observable in the swollen gel, either confined in the pores or included in the walls (Fig. 3*C*). The TC-PN FT3 shows a more intense red fluorescence than FT1 (*SI Appendix*, Fig. S5), suggesting that the amount of L-PVA that remains in the TC-PN after washing increases with the number of FT cycles. This suggests that the ice crystals that form during freezing push the L-PVA droplets onto the continuous H-PVA gel, producing a "force-coating" of the initially microphase separated gel with L-PVA and originating a quasibigel (27).

Overall, passing from pregel solutions to swollen FT gels causes the formation of inhomogeneities also at the nanoscale; this, along with the swelling of PVA chains in water, leads to an increase of the correlation lengths, as evidenced by SAXS (*SI Appendix*, Table S2).

The lower value of the correlation length of TC-PN FT1 as opposed to the PVA FT1 suggested that the spontaneous H-PVA/L-PVA phase separation produces a higher concentration of H-PVA in the continuous phase, which eventually led to the formation of denser gel walls than in the single-polymer network. In fact, the crystallinity of TC-PN gels is higher than the pure PVA network (*SI Appendix*, Table S1 and Fig. S6). In the pure PVA networks, crystallinity increases with increasing FT cycles, as expected (24, 40, 41), while, in the PVA/PVA systems, it stabilizes, confirming that the TC-PN conserves its structure after the first cycle, as discussed under *The Structure of PVA-Based Cryogels*.

The Diffusion of PVA Chains in the Pregel Solutions and Gels. FCS and FRAP were employed to study the mobility of the polymer chains in the PVA and PVA/PVA pregel solutions and gel networks. The two techniques allow measuring different ranges of the diffusion coefficient, ideally $D > 1$ $\mu m^2/s$ for FCS and 0.01 $\mu m^2/s < D < 50$ $\mu m^2/s$ for FRAP (*SI Appendix*, section S2.4).

As expected, the diffusion of the H-PVA chains in the walls of the cryogels is too slow to be detected by FRAP (*SI Appendix*, Fig. S7). While other techniques could be employed to study such slow diffusion rates, e.g., single-particle tracking (42), image correlation spectroscopy (43), or NMR diffusometry (44), for the scopes of this work, it was important to observe that the polymer chains are essentially blocked in the gels' walls, providing an upper limit (0.01 $\mu m^2/s$) for their diffusion coefficients. A qualitative comparison of the FRAP curves (*SI Appendix*, Fig. S7D) shows that in the PVA FT1 network, H-PVA is less strongly blocked than in the TC-PN FT1, indicating that the latter has a more crowded gel structure. When the number of FT cycles increases, the differences between PVA and PVA/PVA level off.

In the PVA/PVA pregel solutions, the chains of H-PVA are less mobile (lower values of D; *SI Appendix*, Fig. S7 and Table S4) than in the single-polymer pregels, in agreement with the gelation process illustrated with confocal microscopy, where the phase separation in the PVA/PVA system causes a concentration increase of H-PVA outside the blobs of L-PVA (Fig. 3).

The most striking observation concerns the mobility of L-PVA in the formed TC-PNs, after curing in water. Inside the gels' pores, the polymer shows two diffusional behaviors, with a predominant component of free polymer (as in diluted solution) and a minor component of slower diffusing chains (Fig. 4 *A–C* and *SI Appendix*, Table S4). We reasonably hypothesized that the slow-diffusing components are constituted by L-PVA chains that are not included in the TC-PNs, but interact with them through hydrogen bonds, or are chains partially protruding out of the walls. Instead, the L-PVA chains on the walls of the TC-PNs are strongly blocked and do not show a diffusional behavior as evidenced by FRAP (Fig. 4D and *SI Appendix*, Table S4). Both the inclusion of L-PVA and its protrusion from the gel walls could also be explained considering the possibility that some "force-coating" of the walls with L-PVA occurs through the FT process, as mentioned above. Overall, we concluded that L-PVA contributes to the structure of the TC-PNs, and this is expected to produce significant changes in the mechanical properties of the PVA/PVA gels as opposed to the single-polymer networks.

Rheological Properties of PVA Gels. Rheological measurements clearly demonstrate the influence of composition and FT cycles on the mechanical properties of the gels. The rheological data were related to the structural characterization reported in the previous sections.

Amplitude sweep curves show that the cross-over between the storage modulus (G′) and loss modulus (G″) can be found at lower oscillation strains for the FT3 hydrogels (arrows in Fig. 5A). The peak that appears in the G″ curves, the "weak strain overshoot" (45), is shifted to lower strains with increasing FT cycles; this behavior can be explained considering that a higher number of cycles
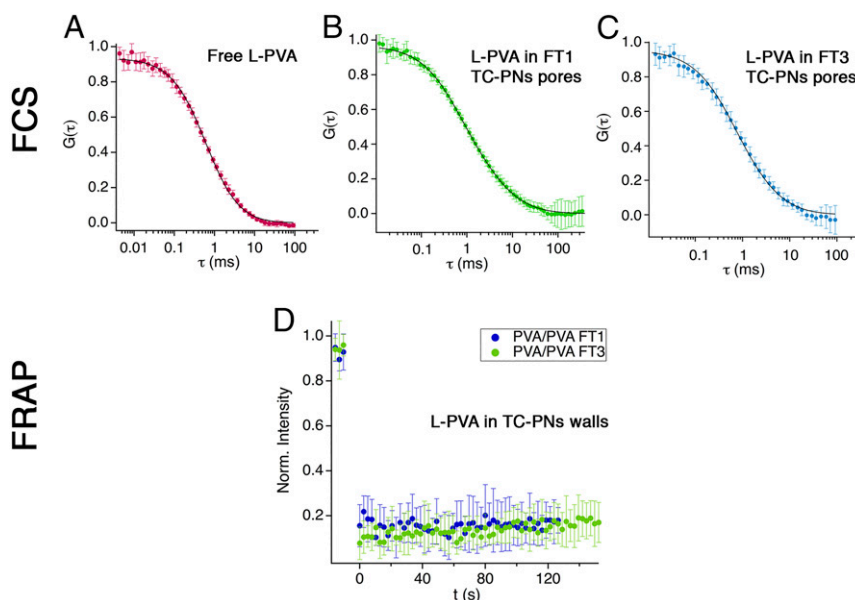

Fig. 4. The diffusion of L-PVA in the TC-PN gels. (*Top*) FCS autocorrelation curves (marks) and fitting functions (solid lines) for a diluted solution of L-PVA in water (*SI Appendix*) (A), L-PVA in the pores of TC-PN FT1 gel (B), and L-PVA in the pores of TC-PN FT3 gel (C). The results of the fittings (values of the diffusion coefficient, D) are reported in *SI Appendix*, Table S4. (D) FRAP recovery profiles of L-PVA on the walls of TC-PN FT1 (blue markers) and FT3 (green markers) gels; the curves are flat, without recovery in the fluorescence intensity, which indicates that no diffusion of the polymer chains is detectable (*SI Appendix*, section S2.3).

leads to stiffer and less mobile networks that are less capable of relaxing mechanical stresses. For the same number of FT cycles, TC-PNs show G″ peaks at higher strain. It can be thus hypothesized that the presence of L-PVA chains included in the gel walls make the final structure more compliant. However, it must be considered that the observed changes in rheological properties could also be due to the morphological differences (e.g., larger and less-oriented pores) induced by templating from L-PVA droplets during gelation.

After one cycle, the TC-PN has a higher G′ than the single-polymer network, as shown in the frequency sweep curves reported in Fig. 5B. This seems in contrast to the lower gel fraction, G%, reported in *SI Appendix*, Table S1, as G′ is known to depend on the polymer concentration (46). However, as previously discussed, denser gel walls are formed during gelation of the TC-PN due to the spontaneous H-PVA/L-PVA phase separation in the pregel solution (Fig. 3). This can explain the increase in the storage modulus.

FT3 gels have all similar G′, significantly higher than the FT1 systems, highlighting that polymer accumulate on gel walls during the freezing steps; in the case of TC-PNs, this could be possibly due also to the "force-coating" of the gel walls with L-PVA through repeated FT cycles. Fig. 5C shows visually the increase in the rigidity of the systems with increasing number of cycles. It must be noticed that systems with excessively high storage moduli are not able to adapt to surface irregularities typical of painted artifacts (i.e., ≥1 mm) (20). This is further visualized in *SI Appendix*, Fig. S8, where FT1 PVA gels are compared to a pHEMA/PVP SIPN we previously formulated for the cleaning of artifacts (19, 21) and to a gellan sheet similar to those traditionally employed in

the restoration practice (47). The pHEMA/PVP gels have G′ values of 4 to 5×10^3 Pa (17), roughly half the modulus of a typical gellan sheet (48). In turn, the newly formulated PVA gels have G′ moduli 4 to 5 times lower than those of pHEMA/PVP and still exhibit very good resistance to handling and elongation. Both the pure and TC-PN FT1 PVA gels are able to adapt to the rough painted surface, covering irregularities and insinuating into cavities (*SI Appendix*, Fig. S8 *D and E*), whereas the pHEMA/PVP SIPN and gellan sheet are too rigid to cover the surface homogeneously (*SI Appendix*, Fig. S8 *B and C*). This is expected to boost the cleaning efficacy of the PVA gels. Being more compliant than the pure PVA network, the H-PVA/L-PVA gel might adhere better to the painted surface, producing a more homogeneous cleaning. Moreover, given that L-PVA is hydrolyzed to a lesser degree than H-PVA, a coating of L-PVA on the surfaces of the pores could result in a material that more efficiently adsorbs hydrophobic particles, enhancing particle uptake.

Removing Dirt from Pollock's Masterpieces. As reported in *SI Appendix*, Table S1, all of the PVA-based gels contain high percentages of water (>90%), which behaves almost completely as free water and is responsible for effective cleaning action. In fact, water is a good solvent for the surface dirt commonly found on artifacts, and its cleaning power is easily enhanced when solutions of chelants or surfactants are used. Besides, as reported in *SI Appendix*, Table S1, the water release of the PVA-based formulations reported here is in the range of 21 to 24 mg/cm^2 (over 30 min, on Whatman paper) for FT1 gels and 17 to 19 mg/cm^2 for FT3 gels. These values are comparable with those of pHEMA/PVP gels used
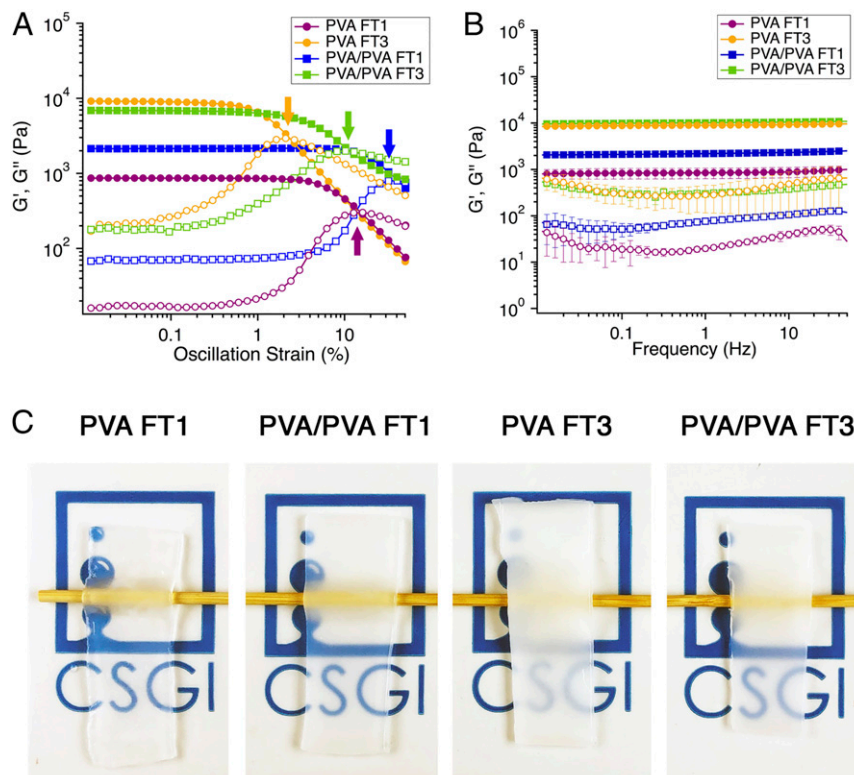

Fig. 5. Rheological measurements and visual aspect of cryogels. (*A*) Amplitude sweep curves of cryogels; the arrows indicate the cross-over of G′ and G″ in different systems. Solid and empty markers indicate G′ and G″, respectively. The oscillation strains at the cross-over follow the trend: PVA FT3 < PVA/PVA FT3 ~ PVA FT1 < PVA/PVA FT1. Error bars are not included to facilitate the readability of the image (*SI Appendix*); errors do not affect cross-over trend. (*B*) Frequency sweeps of cryogels. Solid and empty markers indicate G′ and G″, respectively. Error bars show the SDs; when not visible, they are smaller than the markers' size. (*C*) Cryogels on wooden sticks and colored logos. The increase in the number of cycles leads to opaquer and more rigid systems. CSGI, Consorzio Interuniversitario per lo Sviluppo dei Sistemi a Grande Interfase (Center for Colloid and Surface Science).

for restoration, i.e., 15 to 16 mg/cm^2 (49), and both formulations are more retentive than traditional agar or gellan (30–33 mg/cm^2; ref. 49), which proved too risky to water-sensitive dyes (19). These features, combined with the ability to adapt to rough surfaces, indicate PVA gels as good candidates for the cleaning of sensitive painted layers, based on the background we acquired on the application of gels to the cleaning of artifacts (19, 20, 50). The gels were practically assessed on soiled glass slides (*SI Appendix,* Fig. S9) and on representative mockups that mimic modern/contemporary paintings (*SI Appendix,* Fig. S10) and were compared with conventional cleaning tools such as gellan sheets and swabs (Figs. 6 and 7). The soil was efficiently removed from glass slides and from the rough painted surface using the TC-PN (Fig. 6*E* and *SI Appendix,* Fig. S9), while only partial cleaning was achieved using the pure PVA gel (Fig. 6*D* and *SI Appendix,* Fig. S9). Scarce soil removal was obtained using the gellan sheet (Fig. 6*F*), as expected considering the poor adhesion of the rigid sheet to the clotted painted surface.

Fig. 7 shows that, when the swabs (soaked with the same cleaning solution as gels) are used, repeated mechanical action and scarce water retentiveness inevitably causes pigment loss. Instead, the application of TC-PNs leads to the safe removal of the soil; softened soil residues are easily removed via gentle mechanical action with an "eraser gum"-shaped TC-PN without detaching the pigment from the surface (Fig. 7*A*).

Two-dimensional (2D) Fourier-transform infrared spectroscopy (FTIR) imaging allowed assessment of the gel-cleaning effectiveness down to the micron scale. The spectra of the cleaned sample are comparable to those of the pristine mockup (Fig. 7*B*), mainly showing the peaks of oil paintings (51). The bands of kaolin in the 3,725 to 3,592 cm^{-1} region (3,665 cm^{-1}, Al–OH stretching; 3,625 cm^{-1}, OH stretching, crystalline hydroxyl) (52) are intense in the spectra of the soiled mockup and absent in those of the pristine and cleaned samples, indicating effective soil removal. Previously,

we had shown that conventional rigid gels have poor adhesion to such rough surfaces, resulting in scarce removal of soil (20).

Besides, mapping the absorbance intensity in the PVA OH stretching region (3,440 to 3,180 cm^{-1}) showed no significant differences between the pristine and cleaned samples; no absorption bands ascribable to PVA could be detected (Fig. 7*C*), i.e., no residues of PVA were left on the surface (up to the detection limit of ca. 0.02 pg/μm^2; *SI Appendix,* Fig. S11 and section S2.5). This was deemed as a fundamental feature, as opposed to traditional thickeners (e.g., polyacrylic acid, cellulose ethers); the latter are known to leave residues after cleaning and require detrimental rinsing steps (9, 53, 54).

The TC-PN FT1 hydrogels were then used to clean two Jackson Pollock masterpieces at the Peggy Guggenheim Collection (Venice), namely "Eyes in the Heat" (1946 to 1947) and "Two" (1943 to 1945), jeopardized by surface dirt accumulated over the last decades (Fig. 8). These artifacts are particularly important in the Pollock oeuvre, showing the transition from a relatively traditional language, to the revolutionary dripping technique that produces textured 3D surfaces. Moreover, "Two" is made using only oil paints, while "Eyes in the Heat" represents the artist's transition from oil paints to the application of both oils and alkyd colors. In both cases, the painted surface is highly solvent sensitive. These combined features make the removal of dirt particularly challenging and risky with conventional cleaning tools.

The removal of soil using the gels is appreciated as the paints' hue is brought back (Fig. 8 *A* and *D*). The gels' mechanical properties and retention/release rate allowed feasible dirt removal without unwanted effects, whereas swabs were shown to remove pigments along with dirt and were thus avoided. Because dirt removal takes place through controlled wetting and dirt detachment at the gel–paint interface, rather than via traditional solution chemistry, the systems reported here allow safe cleaning. Therefore, the length of the cleaning intervention was optimized as opposed to
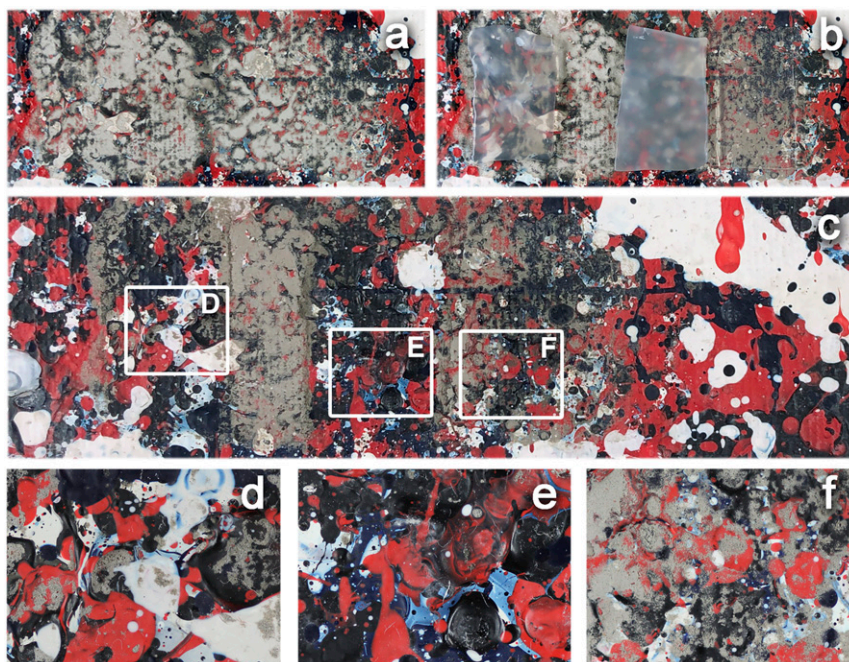
Fig. 6. Cleaning tests on mockups: assessment of PVA and traditional gels. (*A*) Clotted painting mockup that mimics Pollock's alkyd paintings, artificially soiled. (*B*) Application of a pure PVA FT1 gel (*Left*), a PVA/PVA FT1 TC-PN (*Center*), and a gellan gel sheet similar to those used in the traditional restoration practice (*Right*). (*C*) Soil removal after the application of the gels (8 min each); no additional mechanical action was carried out after the removal of the gels. *D*–*F* detail the removal efficacy of each type of gel: the soil was efficiently removed using the TC-PN (*E*), while partial cleaning was achieved using the pure PVA gel (*D*). Scarce soil removal was obtained using the gellan sheet (*F*), as expected considering the poor adhesion of the rigid sheet to the clotted painted surface. *A* and *B* represent areas of 9.5× 4.1 cm^2. *C* has a magnification of 1.25×. *D*–*F* have magnification of 3.4× with respect to *A* and *B*, and are magnifications of *Insets* (*D*–*F*) in *C*.
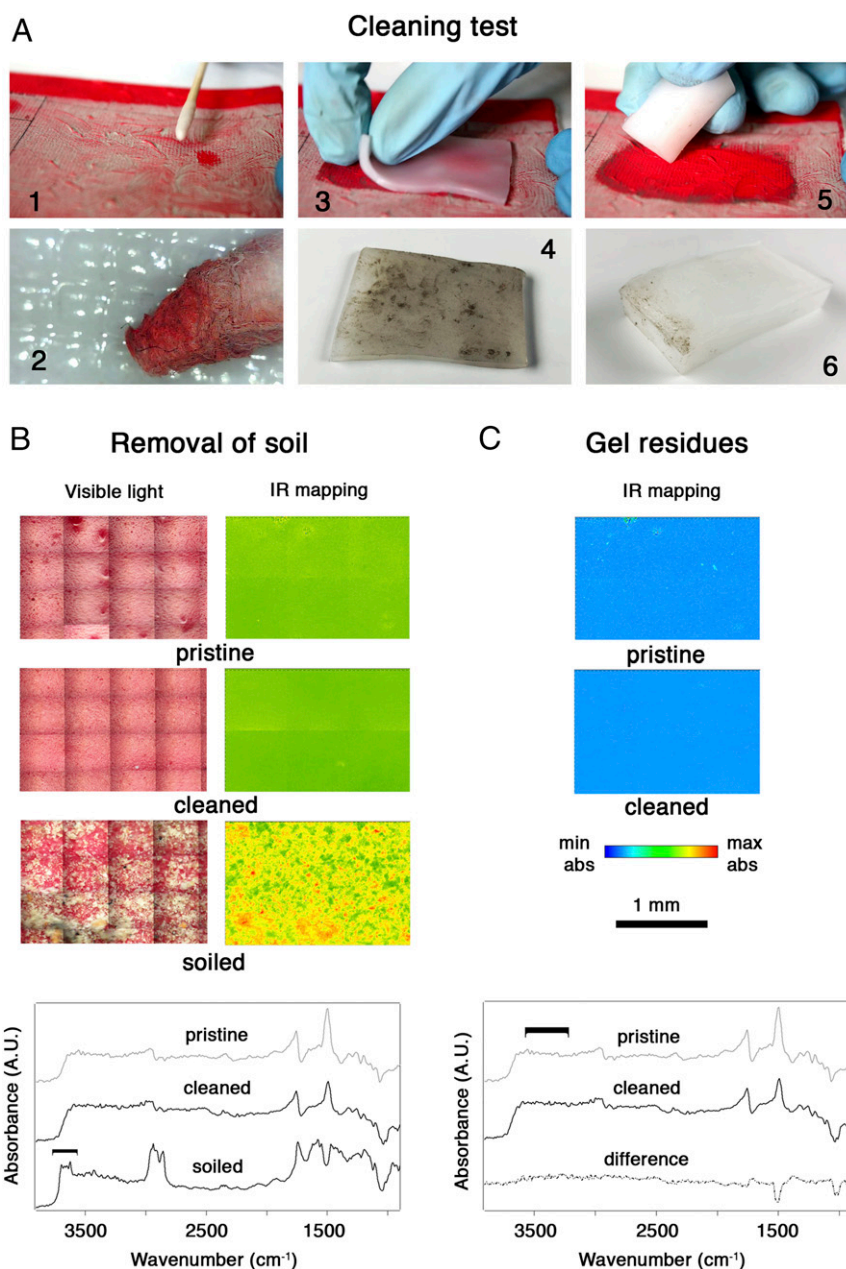
Fig. 7. Cleaning tests on mockups: assessment of the cleaning using FTIR 2D Imaging. (*A*) Removal of artificial soil from an oil painting mockup (water sensitive cadmium red color) that mimics Pollock paintings (*1*, *2*). Removal using a swab soaked with a cleaning aqueous solution. The detail in *2* shows the removal of some red pigment along with the soil (*3*, *4*). Application of the TC-PN FT1 hydrogel sheet on the soiled surface (i.e., approach proposed in this contribution); *4* shows that only soil, and no red pigment, adheres to the gel sheet following the application (*5*, *6*). The cleaning is completed using the TC-PN FT1 hydrogel shaped as an eraser gum; gentle mechanical action with the gel leads to the complete removal of the soil. The detail in *6* shows that no red pigment adheres to the eraser gum. (*B*) Assessment of the cleaning effectiveness of the TC-PNs hydrogel using FTIR 2D Imaging. The IR maps show the imaging of the bands of kaolin (present in the artificial soil mixture) in the 3,725 to 3,592 cm^{-1} region. (*Top*) Pristine painted surface. (*Center*) Painted surface that was soiled and then cleaned using the TC-PN gel. (*Bottom*) Soiled painted surface. Representative spectra of the pristine, cleaned, and soiled surfaces are shown below the maps. (*C*) Assessment of the absence of gel residues. The IR maps (acquired on the same areas as panel b) show the imaging of the 3,440 to 3,180 cm^{-1} region, where characteristic bands of PVA would be found in case of gel residues after cleaning. (*Top*) Pristine painted surface. (*Bottom*) Painted surface that was soiled and then cleaned using the TC-PN gel. Representative spectra of the pristine and cleaned surface are shown below the maps, along with the difference between the two spectra, showing no absorptions ascribable to PVA. abs, absorbance; max, maximum; min, minimum.

the traditional approach that sometimes involves working with nonconfined solvents under the microscope. Thanks to their mechanical properties and effective solvent confinement, these gels are promising tools in order to obtain a safe and noninvasive action, reducing the actual risks for the painted surface, i.e., swelling, solubilization, leaching, and unwanted removal of fatty acids, plasticizers, and metal soaps.

Conclusions

FT gels entirely based on PVA were specifically designed to address the challenge of dirt removal from solvent-sensitive artistic surfaces. At the micron scale, pure PVA networks show an ordered pore structure, with elongated and oriented pores. Instead, TC-PNs exhibit a sponge-like disordered and interconnected macroporosity, with larger pores and increased surface roughness,
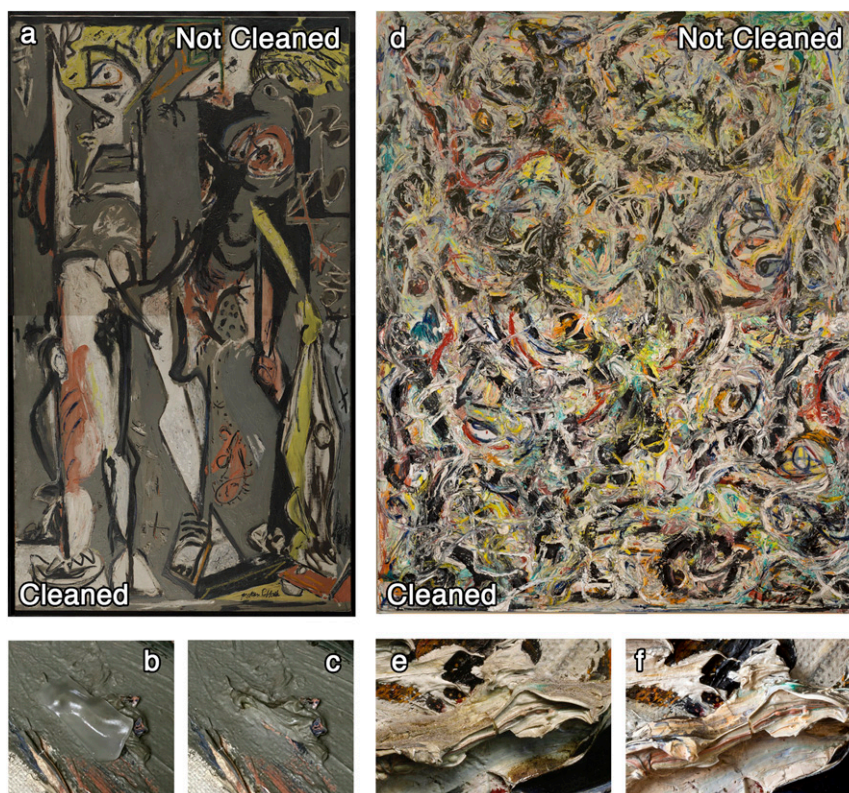
Fig. 8. Cleaning of Pollock's masterpieces. (*Left*) *Two* by Jackson Pollock, © Pollock-Krasner Foundation/Artists Rights Society (ARS), New York. (*Right*) *Eyes in the Heat* by Jackson Pollock, © Pollock-Krasner Foundation/Artists Rights Society (ARS), New York. (*A and D*) Collages showing the paintings before and after the cleaning intervention, where the soil was removed using the TC-PN FT1 hydrogels. The collages allow to better appreciate the removal of soil as the paints' hue and brightness were brought back. The whole paintings were cleaned during the cleaning intervention. (*B and C*) A detail showing the gel adhering to the painting and the same area after cleaning. (*E and F*) A detail of the painting before and after cleaning with the TC-PN gels. *B* and *C* have a magnification of 13× with respect to *A*. *E* and *F* have a magnification of 20× with respect to *D*.

which were shown to enhance the capture of dirt at the gel–paint interface and its inclusion in the gels.

The TC-PNs exhibit higher storage modulus but better relief of mechanical stress than the pure PVA networks, possibly as a result of the plasticizing action of L-PVA or of the morphological changes induced by templating from L-PVA droplets during gelation. Remarkably, these gels behave mechanically as chemical networks, despite being held by noncovalent bonds.

TC-PNs were used to safely remove dirt from the surface of Jackson Pollock's masterpieces, "Two" and "Eyes in the Heat." Thanks to their adhesion to the textured surface, to the controlled release of cleaning fluids at the gel–paint interface, and to the enhanced removal of dirt, the TC-PNs allowed the cleaning of the artifacts without undesired effects on sensitive painted layers, overall optimizing the cleaning process. TC-PNs offer innovative solutions to several needs in cleaning of modern and contemporary paintings in terms of dirt removal, cleaning selectivity, decreased impact on the painted surface, and accuracy of the intervention.

The results presented here are an important step forward in the field of conservation of cultural heritage, opening to feasible treatment of important sets of artifacts, granting their transfer to future generations, with a vast potential socioeconomic impact.

Materials and Methods

Hydrogel Preparation. PVA-based cryogels were prepared through one or three FT cycles starting from PVA solutions. After the last thawing step, gel samples were stored in demineralized water for 1 wk.

Hydrogel Characterization. Hydrogel structure was characterized with confocal laser scanning microscopy, SEM, and SAXS. The mechanical properties were studied with rheological measurements (amplitude and frequency sweeps). Crystallinity degree, equilibrium water content, and free water index were measured using derivative thermogravimetry and differential scanning calorimetry. FCS and FRAP were used to study the dynamics of the PVA chains in the hydrogels' network.

Painting Mockups. Painting mockups were prepared using a commercial primed canvas, oil (Windsor & Newton), and alkyd colors (Ferrario). After about 1 y from the preparation, an artificial dirt mixture in ligroin was applied by means of a brush over the paint layer.

Cleaning Trials. The hydrogels were applied on the surface of soiled mockups for 1 min. The cleaning was completed by gentle mechanical action using an "eraser gum"-shaped hydrogel. The cleaning effectiveness and the absence of PVA residues on the treated surfaces were checked using 2D FTIR imaging with an focal-plane array detector. The same cleaning protocol was adopted for the removal of soil from "Two" and "Eyes in the Heat" by Jackson Pollock. Full methods and materials are available in *SI Appendix*.

Data and Materials Availability. All data are available in the main text or *SI Appendix*.

1. C. Dümcke, M. Gnedovsky, "The social and economic value of cultural heritage: Literature review" (European Expert Network on Culture Paper, Interarts Foundation, 2013).

2. N. Stanley-Price, "The thread of continuity: Cultural heritage in post-war recovery" in *Cultural Heritage in Postwar Recovery: Papers from the ICCROM FORUM Held on October 4–6, 2005* (International Center for the Study of the Preservation and Restoration of Cultural Property, 2007), pp. 1–16.

3. C. Holtorf, The changing contribution of cultural heritage to society. *Mus. Int.* **63**, 8–16 (2011).

4. T. J. S. Learner, "The chemistry of modern paints" in *Analysis of Modern Paints* (Getty Conservation Institute, 2004), pp. 12–13.

5. F. C. Izzo, K. J. van den Berg, H. van Keulen, B. Ferriani, E. Zendri, "Modern oil paints–Formulations, organic additives and degradation: Some case studies" in *Issues in Contemporary Oil Paint*, K. J. Van der Berg *et al.*, Eds. (Springer International Publishing, 2014), pp. 75–104.

6. A. Burnstock, K. J. van den Berg, S. de Groot, L. Wijnberg, "An investigation of water-sensitive oil paints in 20th century paintings" in *Modern Paints Uncovered: Proceedings from the Modern Paints Uncovered Symposium*, T. J. S. Learner, P. Smithen, J. Krueger, M. R. Shilling, Eds. (The Getty Conservation Institute, 2007), pp. 177–188.

7. B. Ormsby, T. Learner, The effects of wet surface cleaning treatments on acrylic emulsion artists' paints–A review of recent scientific research. *Stud. Conserv.* **54**, 29–41 (2009).

8. E. Carretti, R. Giorgi, "Cleaning IV: Applications and case studies" in *Nanoscience for the Conservation of Works of Art*, P. Baglioni, D. Chelazzi, Eds. (Royal Society of Chemistry, 2013), pp. 287–288.

9. A. Casoli, Z. Di Diego, C. Isca, Cleaning painted surfaces: Evaluation of leaching phenomenon induced by solvents applied for the removal of gel residues. *Environ. Sci. Pollut. Res. Int.* **21**, 13252–13263 (2014).

10. P. Baglioni, E. Carretti, D. Chelazzi, Nanomaterials in art conservation. *Nat. Nanotechnol.* **10**, 287–290 (2015).

11. P. Baglioni, D. Chelazzi, R. Giorgi, G. Poggi, Colloid and materials science for the conservation of cultural heritage: Cleaning, consolidation, and deacidification. *Langmuir* **29**, 5110–5122 (2013).

12. D. Chelazzi, R. Giorgi, P. Baglioni, Microemulsions, micelles, and functional gels: How colloids and soft matter preserve works of art. *Angew. Chem. Int. Ed. Engl.* **57**, 7296–7303 (2018).

13. E. Carretti, L. Dei, C. Miliani, P. Baglioni, "Oil-in-water microemulsions to solubilize acrylic copolymers: Application in cultural heritage conservation" in *Progress in Colloid and Polymer Science*, P. Koutsoukos, Ed. (Springer, 2001), pp. 63–67.

14. M. Baglioni, D. Berti, J. Teixeira, R. Giorgi, P. Baglioni, Nanostructured surfactant-based systems for the removal of polymers from wall paintings: A small-angle neutron scattering study. *Langmuir* **28**, 15193–15202 (2012).

15. M. Baglioni *et al.*, Polymer film dewetting by water/surfactant/good-solvent mixtures: A mechanistic insight and its implications for the conservation of cultural heritage. *Angew. Chem. Int. Ed. Engl.* **57**, 7355–7359 (2018).

16. M. Baglioni *et al.*, Nanomaterials for the cleaning and pH adjustment of vegetable-tanned leather. *Appl. Phys. A Mater. Sci. Process.* **122**, 114 (2016).

17. M. Baglioni *et al.*, Complex fluids confined into semi-interpenetrated chemical hydrogels for the cleaning of classic art: A rheological and SAXS study. *ACS Appl. Mater. Interfaces* **10**, 19162–19172 (2018).

18. R. Mastrangelo, C. Montis, N. Bonelli, P. Tempesti, P. Baglioni, Surface cleaning of artworks: Structure and dynamics of nanostructured fluids confined in polymeric hydrogel networks. *Phys. Chem. Chem. Phys.* **19**, 23762–23772 (2017).

19. J. A. L. Domingues *et al.*, Innovative hydrogels based on semi-interpenetrating p-(HEMA)/PVP networks for the cleaning of water-sensitive cultural heritage artifacts. *Langmuir* **29**, 2746–2755 (2013).

20. N. Bonelli, G. Poggi, D. Chelazzi, R. Giorgi, P. Baglioni, Poly(vinyl alcohol)/poly(vinyl pyrrolidone) hydrogels for the cleaning of art. *J. Colloid Interface Sci.* **536**, 339–348 (2019).

21. N. Bonelli, C. Montis, A. Mirabile, D. Berti, P. Baglioni, Restoration of paper artworks with microemulsions confined in hydrogels for safe and efficient removal of adhesive tapes. *Proc. Natl. Acad. Sci. U.S.A.* **115**, 5932–5937 (2018).

22. N. A. Peppas, S. R. Stauffer, Reinforced uncrosslinked poly (vinyl alcohol) gels produced by cyclic freezing-thawing processes: A short review. *J. Control. Release* **16**, 305–310 (1991).

23. N. A. Peppas, D. Tennenhouse, Semicrystalline poly(vinyl alcohol) films and their blends with poly(acrylic acid) and poly(ethylene glycol) for drug delivery applications. *J. Drug Deliv. Sci. Technol.* **14**, 291–297 (2004).

24. V. I. Lozinsky, L. G. Damshkaln, I. N. Kurochkin, I. I. Kurochkin, Study of cryostructuring of polymer systems: 28. Physicochemical properties and morphology of poly(vinyl alcohol) cryogels formed by multiple freezing-thawing. *Colloid J.* **70**, 189–198 (2008).

25. P. Levitz, D. Tchoubar, Disordered porous solids: From chord distributions to small angle scattering. *J. Phys. I* **2**, 771–790 (1992).

26. P. Levitz, Toolbox for 3D imaging and modeling of porous media: Relationship with transport properties. *Cement Concr. Res.* **37**, 351–359 (2007).

27. L. Di Michele *et al.*, Multistep kinetic self-assembly of DNA-coated colloids. *Nat. Commun.* **4**, 2007 (2013).

28. N. Limpan, T. Prodpran, S. Benjakul, S. Prasarpran, Influences of degree of hydrolysis and molecular weight of poly(vinyl alcohol) (PVA) on properties of fish myofibrillar protein/PVA blend films. *Food Hydrocoll.* **29**, 226–233 (2012).

29. C. M. Hassan, J. E. Stewart, N. A. Peppas, Diffusional characteristics of freeze/thawed poly(vinyl alcohol) hydrogels: Applications to protein controlled release from multilaminate devices. *Eur. J. Pharm. Biopharm.* **49**, 161–165 (2000).

30. V. I. Lozinsky, L. G. Damshkaln, Study of cryostructuration of polymer systems. XVII. Poly(vinyl alcohol) cryogels: Dynamics of the cryotropic gel formation. *J. Appl. Polym. Sci.* **77**, 2017–2023 (2000).

31. K. Pal, A. K. Banthia, D. K. Majumdar, Polyvinyl alcohol–gelatin patches of salicylic acid: Preparation, characterization and drug release studies. *J. Biomater. Appl.* **21**, 75–91 (2006).

32. B. J. Pae *et al.*, Phase behavior in PVA/water solution : The coexistence of UCST and LCST. *Korea Polym. J.* **5**, 126–130 (1997).

33. H.-G. Elias, "Solution thermodynamics" in *Macromolecules* (Springer, 1977), p. 233.

34. N. J. Crowther, D. Eagland, The volumetric behaviour of poly(vinyl alcohol) in aqueous solution. *J. Chem. Soc. Faraday Trans. 1* **82**, 2791–2799 (1986).

35. B. M. Budhlall *et al.*, Characterization of partially hydrolyzed poly(vinyl alcohol). Effect of poly(vinyl alcohol) molecular architecture on aqueous phase conformation. *Macromolecules* **36**, 9477–9484 (2003).

36. V. I. Lozinsky *et al.*, Study of cryostructurization of polymer systems VII. Structure formation under freezing of poly(vinyl alcohol) aqueous solutions. *Colloid Polym. Sci.* **264**, 19–24 (1986).

37. L. H. Sperling, "Interpenetrating polymer networks: An overview" in *Interpenetrating Polymer Networks*, D. Klempner, L. H. Sperling, L. A. Utracki, Eds. (American Chemical Society Advances in Chemistry, 1994), pp. 3–38.

38. Y. S. Lipatov, T. T. Alekseeva, "Thermodynamics and phase separation in IPNs" in *Phase-Separated Interpenetrating Polymer Networks* (Advances in Polymer Science, Springer, 2007), vol. 208, p. 47.

39. L. Di Michele *et al.*, Aggregation dynamics, structure, and mechanical properties of bigels. *Soft Matter* **10**, 3633–3648 (2014).

40. F. Yokoyama, I. Masada, K. Shimamura, T. Ikawa, K. Monobe, Morphology and structure of highly elastic poly(vinyl alcohol) hydrogel prepared by repeated freezing-and-melting. *Colloid Polym. Sci.* **264**, 595–601 (1986).

41. R. Ricciardi, C. Gaillet, G. Ducouret, F. Lafuma, F. Lauprêtre, Investigation of the relationships between the chain organization and rheological properties of atactic poly(vinyl alcohol) hydrogels. *Polymer* **44**, 3375–3380 (2003).

42. Y. Chen, B. C. Lagerholm, B. Yang, K. Jacobson, Methods to measure the lateral diffusion of membrane lipids and proteins. *Methods* **39**, 147–153 (2006).

43. M. J. Saxton, K. Jacobson, Single-particle tracking: Applications to membrane dynamics. *Annu. Rev. Biophys. Biomol. Struct.* **26**, 373–399 (1997).

44. E. Fischer, R. Kimmich, U. Beginn, M. Möller, N. Fatkullin, Segment diffusion in polymers confined in nanopores: A fringe-field NMR diffusometry study. *Phys. Rev. E* **59**, 4079–4084 (1999).

45. K. Hyun *et al.*, A review of nonlinear oscillatory shear tests: Analysis and application of large amplitude oscillatory shear (LAOS). *Prog. Polym. Sci.* **36**, 1697–1753 (2011).

46. A.-L. Kjøniksen, B. Nyström, Effects of polymer concentration and cross-linking density on rheology of chemically cross-linked poly(vinyl alcohol) near the gelation threshold. *Macromolecules* **29**, 5215–5222 (1996).

47. C. Mazzuca *et al.*, Gellan hydrogel as a powerful tool in paper cleaning process: A detailed study. *J. Colloid Interface Sci.* **416**, 205–211 (2014).

48. C. Mazzuca *et al.*, Cleaning of paper artworks: Development of an efficient gel-based material able to remove starch paste. *ACS Appl. Mater. Interfaces* **6**, 16519–16528 (2014).

49. J. Domingues, N. Bonelli, R. Giorgi, P. Baglioni, Chemical semi-IPN hydrogels for the removal of adhesives from canvas paintings. *Appl. Phys. A* **114**, 705–710 (2013).

50. P. Baglioni, D. Chelazzi, R. Giorgi, "Cleaning of easel paintings" in *Nanotechnologies in the Conservation of Cultural Heritage: A Compendium of Materials and Techniques* (Springer, 2015), pp. 83–116.

51. C. Duce *et al.*, FTIR study of ageing of fast drying oil colour (FDOC) alkyd paint replicas. *Spectrochim. Acta A Mol. Biomol. Spectrosc.* **130**, 214–221 (2014).

52. B. J. Saikia, G. Parthasarathy, Fourier transform infrared spectroscopic characterization of kaolinite from Assam and Meghalaya, Northeastern India. *J. Mod. Phys.* **01**, 206–210 (2010).

53. A. Burnstock, R. White, "A preliminary assessment of the aging/degradation of Ethomeen C-12 residues from solvent gel formulations and their potential for inducing changes in resinous paint media" in *Tradition and Innovation: Advances in Conservation: Contributions to the Melbourne Congress, 10–14 October 2000*, A. Roy, P. Smith, Eds. (International Institute for Conservation of Historic and Artistic Work, 2000), pp. 34–38.

54. D. Stulik *et al.*, *Solvent Gels for the Cleaning of Works of Art: The Residue Question*, D. Stulik, V. Dorge, Eds. (The Getty Conservation Institute, J. Paul Getty Trust, 2004).